Experimental and numerical studies of two-dimensional complex plasma crystals

Lénaïc COUËDEL

Laboratoire PIIM, CNRS, Aix-Marseille Université, Marseille, France,
University of Saskatchewan, Saskatoon, Canada.

Online Low Temperature Plasma (OLTP) seminar
13$^{\mathrm{th}}$ August 2024

Collaborators :

- V. Nosenko and group, DLR
- L. Matthews and group, CASPER, Baylor University,
- A. Ivlev and group, MPE,

Department of Physics and Engineering Physics

- Atmospheric and Space Physics
- Magnetic resonance imaging
- Materials science with synchrotron radiation
- Plasma Physics
- Subatomic physics
- Advanced materials

STOR-M tokamak

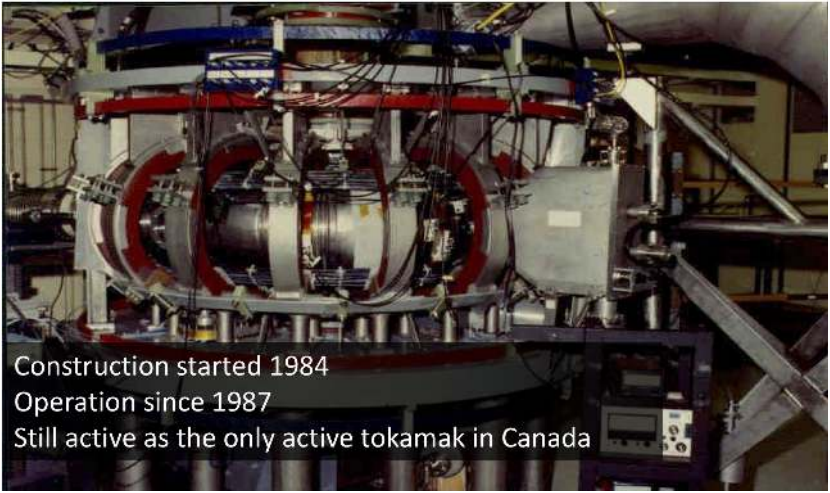

PIIM laboratory at CNRS/Aix-Marseille Université

- Dilute gases
- Plasmas
- Ion beams
- Spectrocopy of atoms and molecules
- Surface interactions

Current research interests

- Low temperature plasma diagnostics (probes, LIF)
- Magnetron sputtering, nanoparticles formation
- Dusty and misty plasmas, plasma crystals
- Simulation of low temperature plasmas (PIC)

Outline

Complex (dusty) plasmas

Monolayer (quasi-2D) complex plasma crystals

Wave modes in monolayer complex plasma crystals

Mode-coupling in 2D plasma crystals

Stability of monolayer complex plasmas : thresholds of MCI, sheath and ion wakes

Summary and Conclusion

Complex (dusty) plasmas

Complex (dusty) plasmas ?

(Partially) ionised gases containing (negativelly) charged solid nano- or micro-particles.

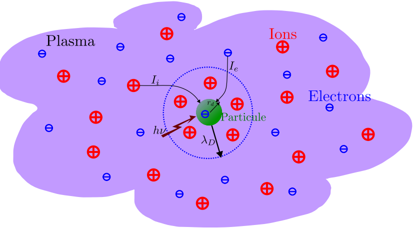

Complex (dusty) plasmas ?

(Partially) ionised gases containing (negativelly) charged solid nano- or micro-particles.

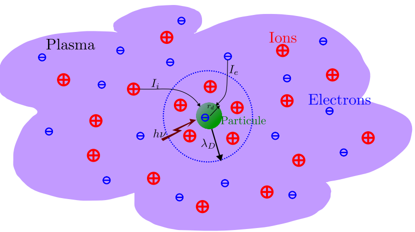

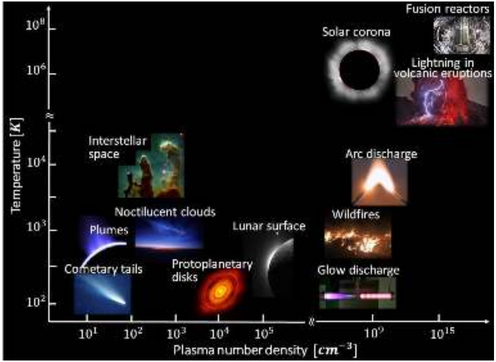

Source : `https://sites.baylor.edu/eva_kostadinova/2019/05/10/__trashed-2__trashed/`

Microparticle electric charge

When a microparticle is immersed in a plasma, it can collect of emit currents :

- electrons,
- ions,
- thermionic emmision,
- UV-induced secondary electrons emission...

In equilibrium :

$$\frac{\mathrm{d}Q_{\mathrm{d}}}{\mathrm{d}t} = \sum_k I_k = 0$$

Microparticle electric charge

When a microparticle is immersed in a plasma, it can collect of emit currents :

- electrons,
- ions,
- thermionic emmision,
- UV-induced secondary electrons emission...

In equilibrium :

$$\frac{\mathrm{d}Q_\mathrm{d}}{\mathrm{d}t} = \sum_k I_k = 0$$

<u>OML theory</u> (Collision-less Maxwellian plasmas) :

Ion and electron currents :

$$I_\mathrm{i} = \pi r_\mathrm{d}^2 n_\mathrm{i} e v_{\mathrm{th_i}} \left(1 - \frac{e\Phi_\mathrm{d}}{k_\mathrm{B} T_\mathrm{i}}\right) \;,$$

$$I_\mathrm{e} = -\pi r_\mathrm{d}^2 n_\mathrm{e} v_{\mathrm{th_e}} \exp\left(\frac{e\Phi_\mathrm{d}}{k_\mathrm{B} T_\mathrm{e}}\right) \;,$$

In equilibrium $|I_\mathrm{i}| = |I_\mathrm{e}|$.

For an isolated particles in an argon plasma :

$$|Z_\mathrm{d}| \simeq 1675 \cdot r_{\mathrm{d},\mu\mathrm{m}} \cdot T_\mathrm{e}(\mathrm{eV}).$$

Monolayer (quasi-2D) complex plasma crystals

How to make a (quasi-)2D plasma crystal ?

Levitation of monosized spherical dust particle in the sheath of a RF discharge.

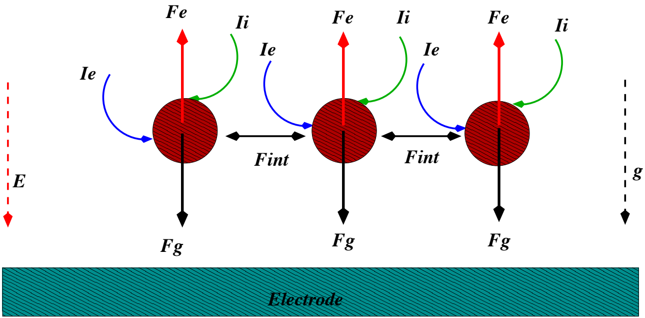

- Weak horizontal confinement
- Strong vertical confinement

Experimental Setup

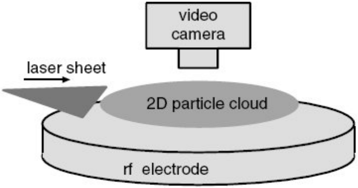

Argon, 0.5 Pa$< p <$ 2 Pa
RF power : 5 W $< P <$ 20 W

Crystallisation of the monolayer

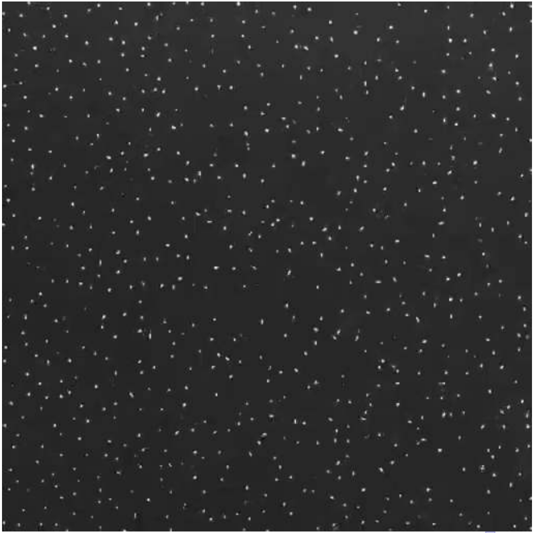

Experimental pictures from a 2D complex plasma crystal

Top view :

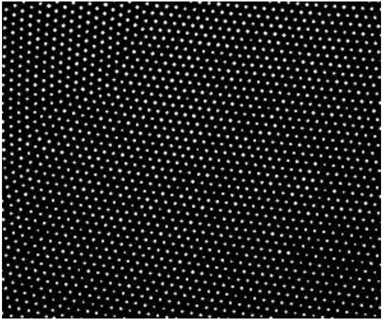

Side view :

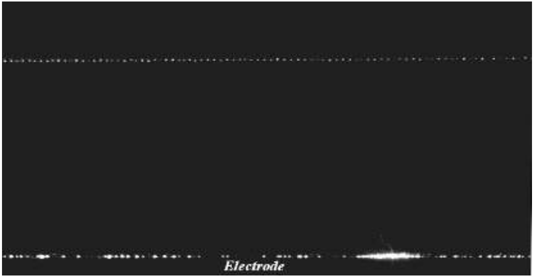

Wave modes in monolayer complex plasma crystals

Interparticle interactions in monolayer complex plasma crystals

- Negatively charged particles in a plasma → Screened-coulomb (Yukawa) interactions.

S. Vladimirov *et al.*, Phys. Plasmas **10**, 3867 (2003)

Interparticle interactions in monolayer complex plasma crystals

- Negatively charged particles in a plasma → Screened-coulomb (Yukawa) interactions.
- In the plasma sheath, strong anisotropy due to ion wakes → Non-reciprocal dust-dust interactions.

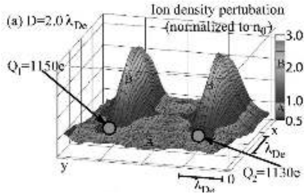

Negligible for strong vertical confinement.

S. Vladimirov *et al.*, Phys. Plasmas **10**, 3867 (2003)

Dynamical matrix and wave modes (Phonons) in 2D crystals

Elementary hexagonal lattice cell :

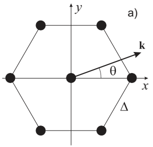

To obtain the eigenfrequencies, we solve :

$$\det[\mathsf{D} - \omega(\omega + i\nu)\mathsf{I}] = 0$$

The dynamical matrix is :

$$\mathsf{D} = \begin{pmatrix} \alpha_\mathrm{h} - \beta & 2\gamma & \\ 2\gamma & \alpha_\mathrm{h} + \beta & \\ & & \Omega^2_\mathrm{conf} - 2\alpha_\mathrm{v} \end{pmatrix}$$

i.e. :

$$(\Omega^2 - \Omega^2_{\mathrm{h}\|})(\Omega^2 - \Omega^2_{\mathrm{h}\perp})(\Omega^2 - \Omega^2_\mathrm{v}) = 0$$

Wave modes in complex plasma crystal

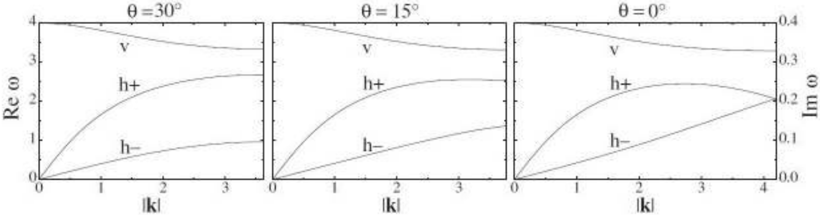

Classic Configuration for particle tracking

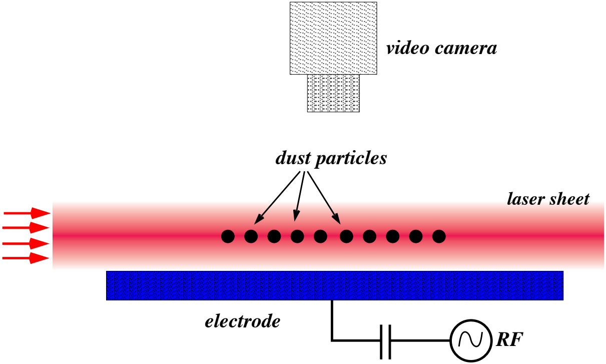

New Configuration for particle tracking (in plane and out of plane motion)

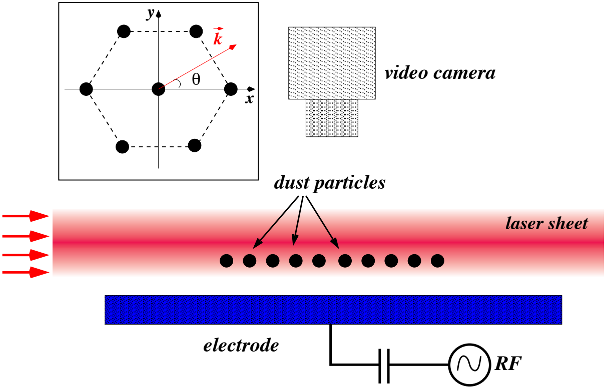

Sensitivity of the configuration to out-of plane motion

In the vertical direction, the laser intensity scale has :

$$I(z) \propto \exp\left(-\frac{(z - z_{max})^2}{2\sigma^2}\right)$$

Standard deviation of laser profile $\sigma \simeq 75\mu$m.
Magnitude of vertical displacement $|\delta z| \sim \sqrt{T_d/m_d\Omega_v^2} \sim 10\mu$m.

Classic configuration :

$z_{lev} \sim z_{max}$

$\delta I/I \sim 1\%$

Negative and positive vertical displacement result in same intensity variations.

New configuration :

$z_{lev} \sim z_{max} - 100\mu$m

$\delta I/I \sim 15\%$

Positive and negative displacement can be resolved.

Scattered intensity variations

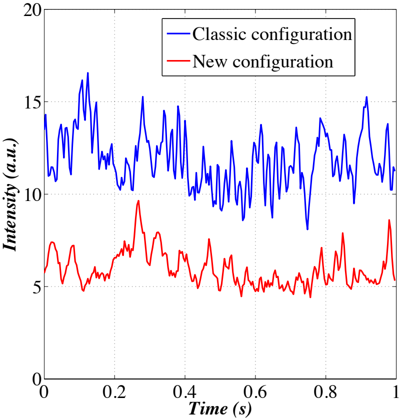

frame rate : 250 fps

Particle diameter : 9.15 μm, p=0.9 Pa, P=5 W

Out of plane fluctuation spectrum

Classic configuration :

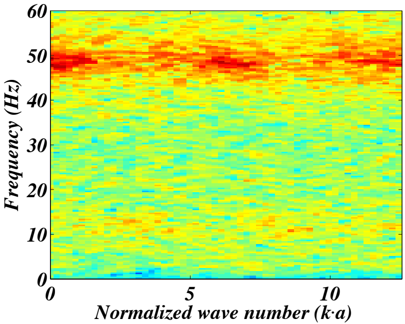

New configuration :

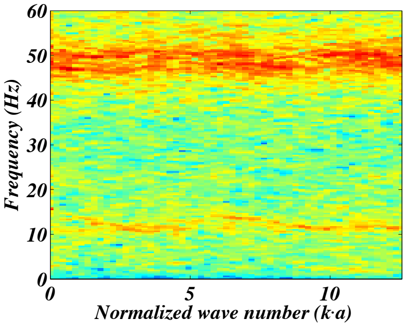

frame rate : 250 fps

Particle diameter : 9.15 μm, p=0.9 Pa, P=5 W

Out-of-plane fluctuation spectrum over a wide range of **k**.

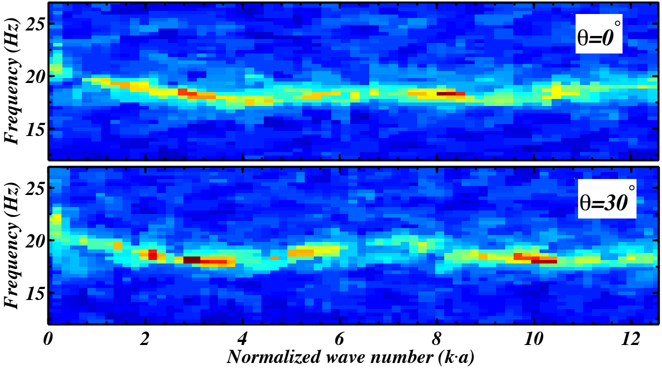

Particle diameter : 8.77 μm, p=0.8 Pa, P=15 W

L.Couëdel *et al.*, Phys. Rev. Lett. **103**, 215001 (2009)

Confirmation of the inverse dispersion relation at long wavelength.
Good agreement with theoretical predictions

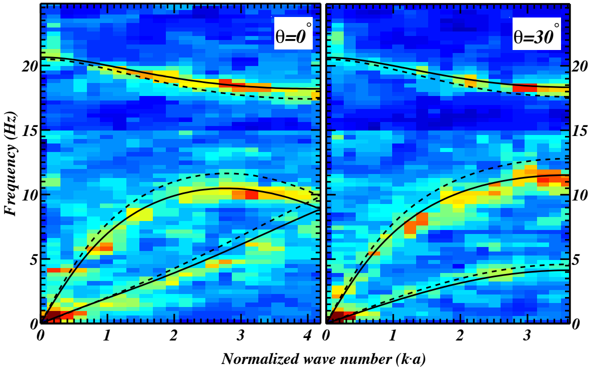

Particle diameter : 8.77 μm, p=0.8 Pa, P=15 W

L.Couëdel *et al.*, Phys. Rev. Lett. **103**, 215001 (2009)

Angular dependence of the fluctuation spectra

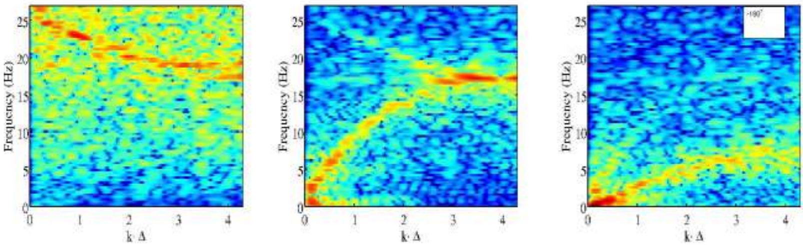

Mode-coupling in 2D plasma crystals

Ion wakes in 2D plasma crystals

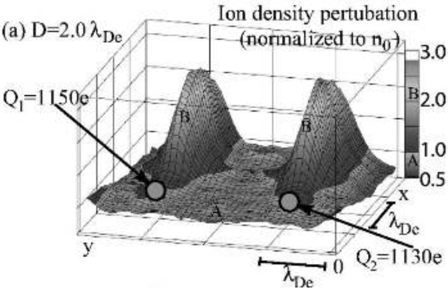

S. Vladimirov *et al.*, Phys. Plasmas **10**, 3867 (2003)

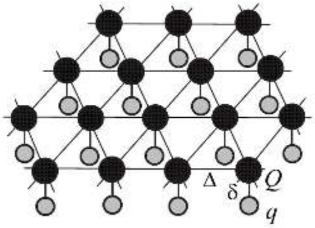

FIG. 1. Sketch illustrating a hexagonal lattice of particles with wakes (oblique view, see text for description).

S.K. Zhdanov *et al.*, Phys. Plasmas **16**, 083706 (2009)

$$\vec{F}_{A\to B} \neq -\vec{F}_{B\to A}$$

Dust-dust interactions are non-reciprocal.

Dynamical matrix and wave modes in 2D crystals

Elementary hexagonal lattice cell :

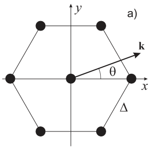

The dynamical matrix is :

$$\mathsf{D} = \begin{pmatrix} \alpha_\mathrm{h} - \beta & 2\gamma & i\sigma_y \\ 2\gamma & \alpha_\mathrm{h} + \beta & i\sigma_x \\ i\sigma_y & i\sigma_x & \Omega^2_\mathrm{conf} - 2\alpha_\mathrm{v} \end{pmatrix}$$

To obtain the eigenfrequencies, we solve :

$$\det[\mathsf{D} - \omega(\omega + i\nu)\mathsf{I}] = 0$$

Without coupling :

$$(\Omega^2 - \Omega^2_{\mathrm{h}||})(\Omega^2 - \Omega^2_{\mathrm{h}\perp})(\Omega^2 - \Omega^2_\mathrm{v}) = 0$$

With coupling :

$$(\Omega^2 - \Omega^2_{h+})(\Omega^2 - \Omega^2_{h-})(\Omega^2 - \Omega^2_{v}) + \Omega^4_{\mathrm{coup}}(\Omega^2 - \Omega^2_{\mathrm{mix}}) = 0$$

S.K. Zhdanov *et al.*, Phys. Plasmas **16**, 083706 (2009)

Hybrid modes in complex plasma crystal

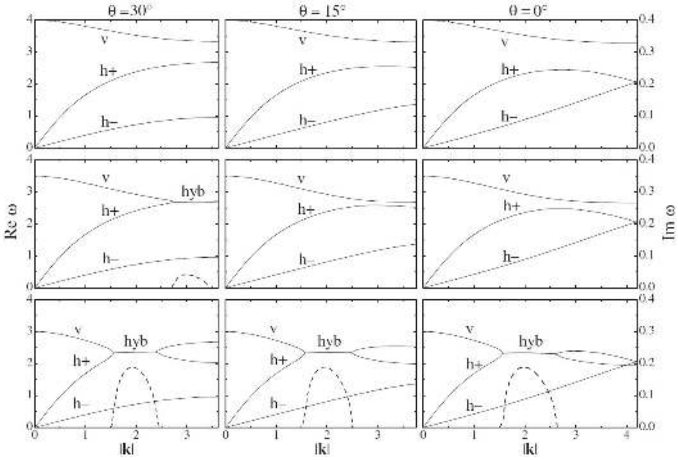

S.K. Zhdanov *et al.*, Phys. Plasmas **16**, 083706 (2009)

Angular dependence (shallow intersection)

Localised heating in the **k**-plane :

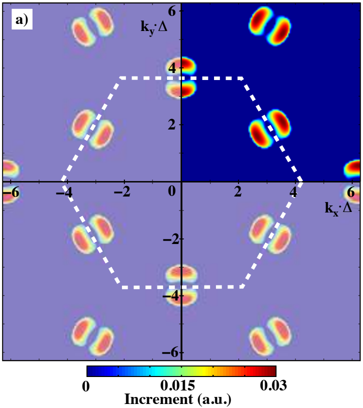

Experimental evidence of the MCI

Experimental evidence of the MCI : Hybrid modes

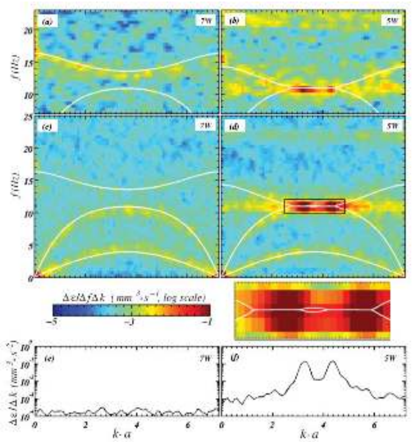

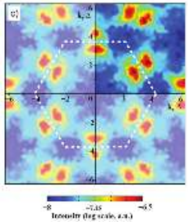

- Formation of the hybrid mode
- Localised heating
- Mixed polarization
- Out-of plane spectrum shows stronger dispersion at small k than the theoretical mode calculated using point-like wake model.

L. Couëdel *et al.*, Phys. Rev. Lett. **104**, 195001 (2010).
L. Couëdel *et al.*, Phys. Plasmas **18**, 083707 (2011).

Mode-coupling induced melting

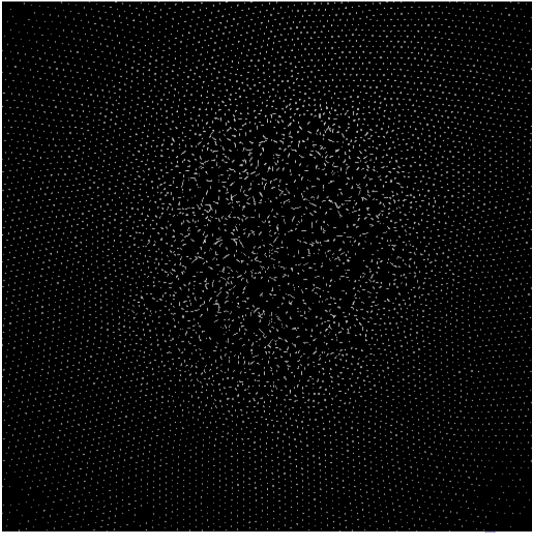

Early stage of the MCI : Synchronisation of particle motion

Mode-coupling induced melting

Top view :

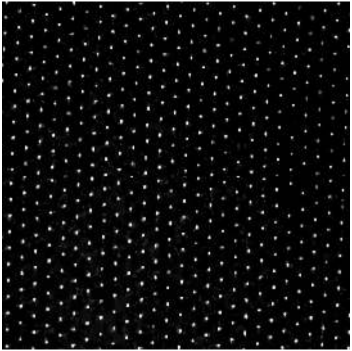

Side view :

RF power : 12 W

Argon pressure : 0.92 Pa
Particle diameter : 9.19 μm.

Particle motion and current spectra

Motion of 2 neighbour particles :

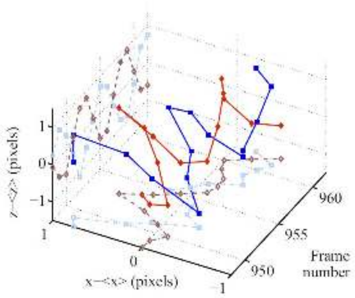

In-plane current fluctuation spectra for different wave propagation angles :

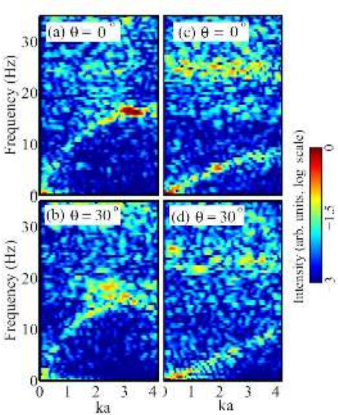

Crystal parameters :
$C_L = (34.1 \pm 1.4)$ mm/s,
$C_T = (7.9 \pm 0.3)$ mm/s.
$a = 480 \pm 10$ μm.
$Q \simeq -18600e$.
$\lambda_D = 380$ μm.
$\kappa \equiv a/\lambda_D = 1.26$.
$f_v = 23 \pm 1$ Hz

Hybrid mode frequency $f_{hyb} = 16 \pm 1$ Hz.

Wave energy distribution in the k-plane around the hybrid mode resonance frequency :
⇒ Instability develops in "most unstable" direction.
⇒ Highly anisotropic oscillations.

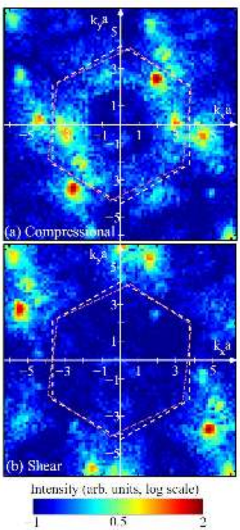

Evolution of the instantaneous phase.

Filtered displacements :

$\tilde{r}_j(t) = r_j(t) - \frac{1}{\Delta t}\int_{t-\frac{\Delta t}{2}}^{t+\frac{\Delta t}{2}} r_j(t')dt'$

Hilbert transform ⇒ instantaneous amplitudes, phases and frequencies.

Synchronisation index :

$\sigma_j = \frac{1}{n}\sum_{j'=1}^{n}\sigma_{jj'}$ with $\sigma_{jj'} = 1 - \frac{S_{jj'}}{S_{max}}$

Shannon entropy of phase distribution $S_{jj'}$:

$S_{jj'} = -\sum_{l=1}^{M} p_{jj'l}\ln p_{jj'l}, \ \sum_{l=1}^{M} p_{jj'l} = 1.$

$p_{jj'l}$: fraction of the data in the l-th bin in the phase difference distribution,

$\phi_{jj'}(t) = \ \phi_j(t) \ - \ \phi_{j'}(t) \ (\mathrm{mod} 2\pi)$,

$l = 1 \ldots M, \ M = 20$

$$\sigma_j = \begin{cases} 1 & \text{synchronised,} \\ 0 & \text{desynchronised.} \end{cases}$$

Evolution of instantaneous phase :

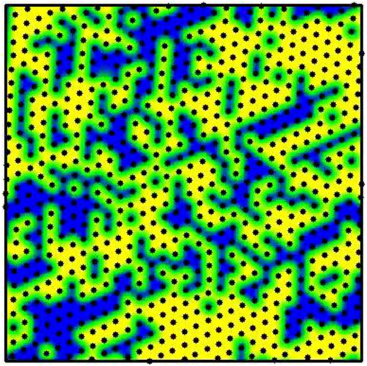

L. Couëdel *et al.*, Phys. Rev. E **89**, 053108 (2014).

Frequency and phase partial synchronisation

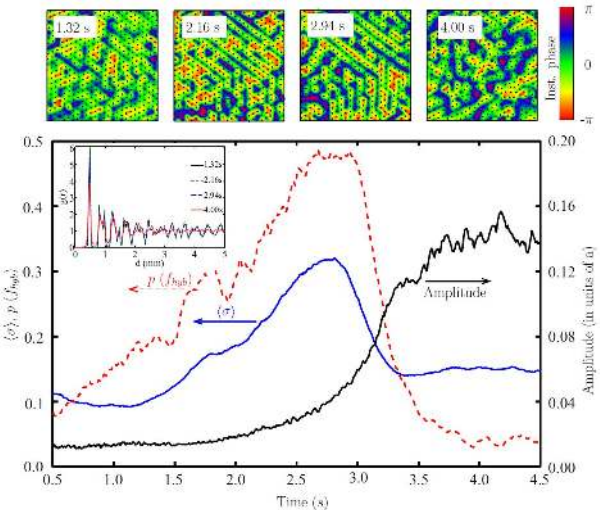

L. Couëdel *et al.*, Phys. Rev. E **89**, 053108 (2014).

Melting and transition to fluid MCI

MCI in fluid 2D complex plasmas

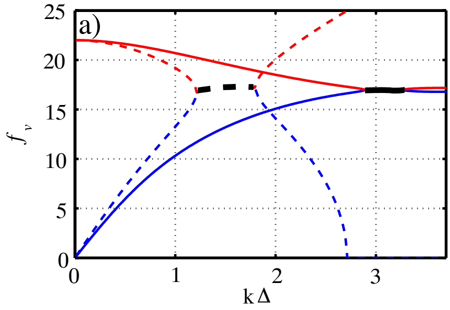

$\kappa = 1.035$, $f_v = 22$ Hz,
Q_d=-18200e, q=0.2$|Q_d|$,
$\Delta = 490\ \mu$m, $\delta = 0.3\Lambda_D$.

A.V. Ivlev *et al.*, Phys. Rev. Lett **113**, 135002 (2014)

- MCI also exists in fluid 2D complex plasmas.
- In fluid, crossing of the mode always occurs
- For the same parameters, growth rate can be higher in the fluid than in the crystal

MCI in fluid 2D complex plasmas

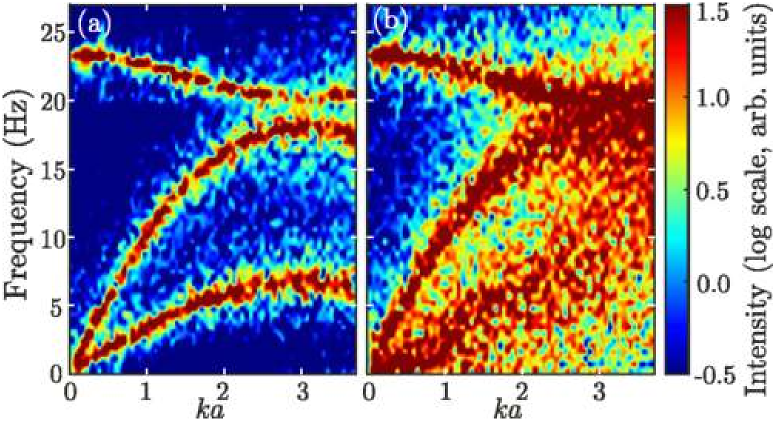

S.O. Yurchenko, et al. Phys. Rev. E **96**, 043201 (2017)

Energy growth during MCI melting

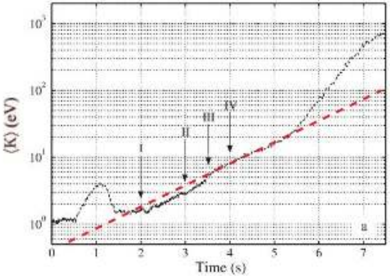

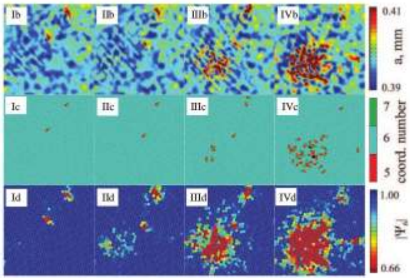

Change of slope when the crystal is melted.

T. B. Röcker *et al.*, Europhysics Letters, **106**, 45001 (2014)

Propagation of the melting front

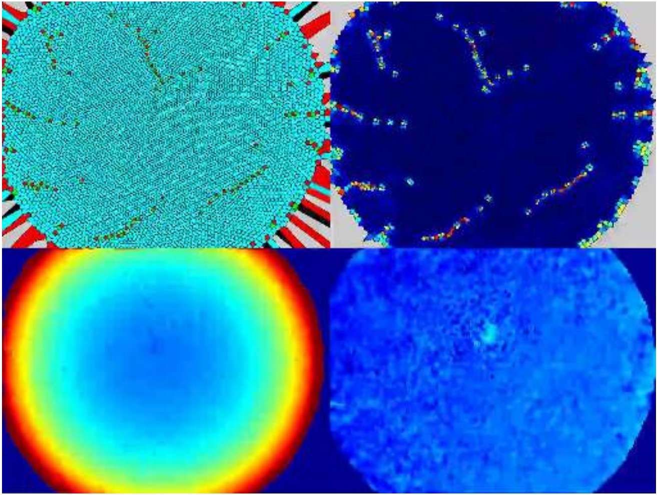

S. O. Yurchenko *et al.*, Phys. Rev. E **96**, 043201 (2017).

Laser-induced explosive melting

Implication of fluid MCI

- Conditions exist for which both the crystalline and the fluid states are viable, meaning no crossing of the modes in the crystal state and MCI growth rate high enough in the fluid state to prevent crystallisation.

Implication of fluid MCI

- Conditions exist for which both the crystalline and the fluid states are viable, meaning no crossing of the modes in the crystal state and MCI growth rate high enough in the fluid state to prevent crystallisation.
- Possibility to trigger sporadic melting of a stable crystal which is not too far from the crystalline MCI threshold by applying a sufficiently strong mechanical perturbation.

Implication of fluid MCI

- Conditions exist for which both the crystalline and the fluid states are viable, meaning no crossing of the modes in the crystal state and MCI growth rate high enough in the fluid state to prevent crystallisation.
- Possibility to trigger sporadic melting of a stable crystal which is not too far from the crystalline MCI threshold by applying a sufficiently strong mechanical perturbation.
- Localised laser stimulation of the monolayer can trigger MCI-induced melting of the stable crystal if the injected energy is sufficient

Experimental set-up

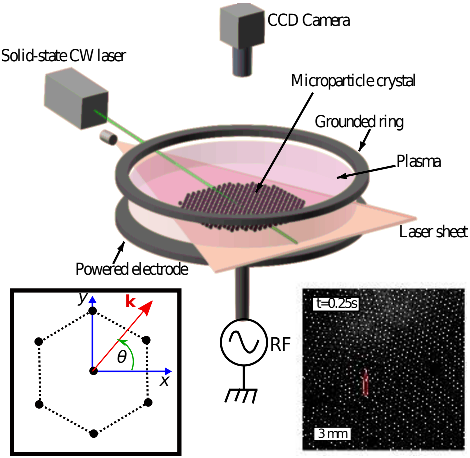

Experimental conditions :

- $P_{\mathrm{Ar}} = 1.04$ Pa
- $P_W = 20$ W
- $\phi_d = 9.19\ \mu$m
- $\Delta = 415 \pm 10\ \mu$m

Stable crystal before laser stimulation

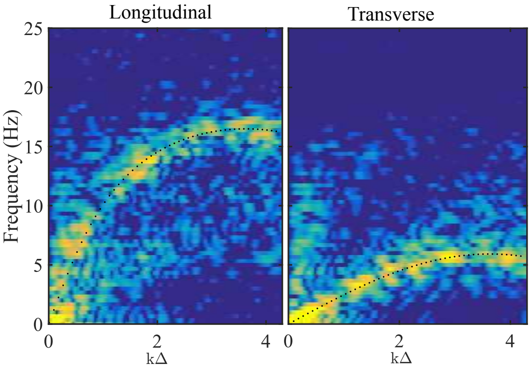

Laser-induced fluid MCI : analogy with thermal runaway in ordinary mater

Laser excitation below threshold :

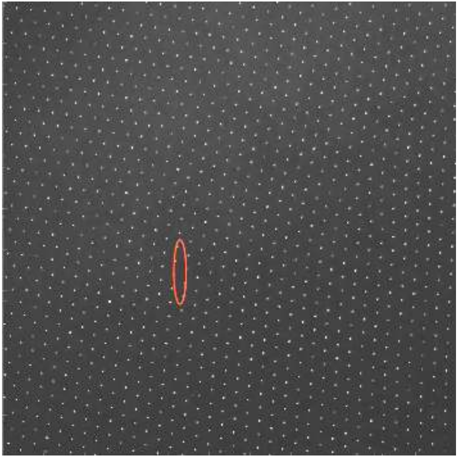

Laser excitation above threshold :

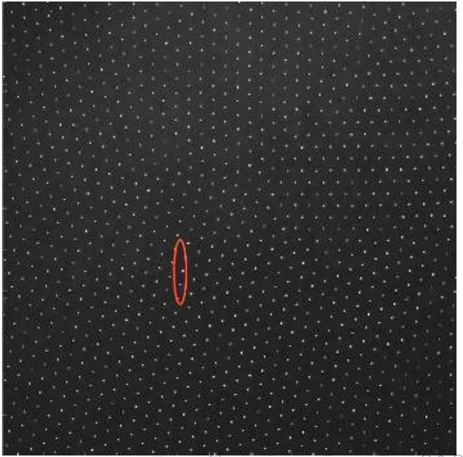

Evolution of the melting spot

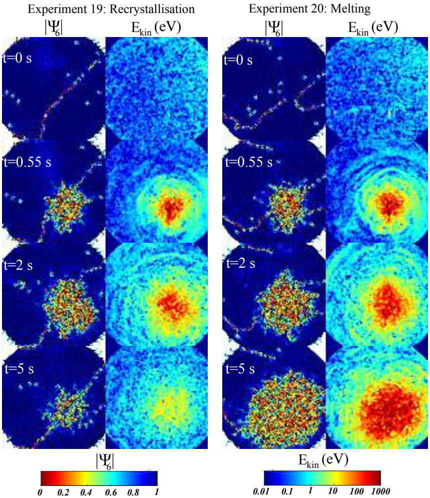

Threshold behaviour

Experiments with different laser pulse energy have been carried out

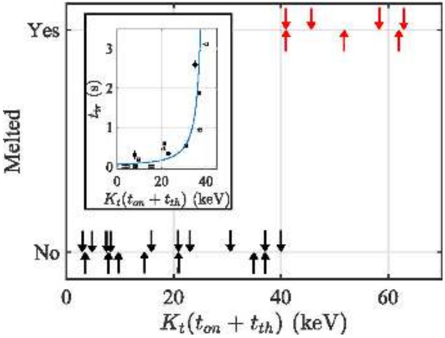

⇒ Full melting occurs only after an injected energy threshold.

Spatial temperature distribution $T(r,t)$ in a continuous reactive medium

The evolution of the kinetic temperature of the microparticles :

$$\frac{\partial T}{\partial t} = \frac{Q(T)}{Cn_{2\mathrm{D}}} - \frac{2\gamma_d}{C}(T - T_0) + \frac{\chi}{r}\frac{\partial}{\partial r}\left(r\frac{\partial T}{\partial r}\right),$$

with the initial condition

$$T(r,0) = T_0 + \frac{E_1}{2\pi w_{\mathrm{MZ}}^2 n_{2\mathrm{D}} C}\exp\left(-\frac{r^2}{2w_{\mathrm{MZ}}^2}\right),$$

The heat source due to fluid MCI :

$$\frac{Q(T)}{Cn_{2\mathrm{D}}} = \frac{\gamma_{\mathrm{MCI}} T_\infty}{C} \mathrm{e}^{-T_a/T},$$

which can be approximated by

$$\frac{Q(T)}{Cn_{2\mathrm{D}}} = \begin{cases} 0, & T < T_a, \\ \frac{\gamma_{\mathrm{MCI}} T_\infty}{C}, & T \geqslant T_a, \end{cases}$$

Spatial temperature distribution $T(r,t)$ in a continuous reactive medium

In dimension-less units the temperature evolution can be written as :

$$\frac{\partial \Theta}{\partial \tau} = \lambda e^{-1/\Theta} - \Gamma\Theta + \frac{1}{\tilde{r}}\frac{\partial}{\partial \tilde{r}}\left(\tilde{r}\frac{\partial \Theta}{\partial \tilde{r}}\right),$$

where $\Theta = T/T_a, \tilde{r} = r/r^*$ with $r^{*2} = E_1/n_{2D}CT_a, \tau = t/t^*$ with $t^* = r^{*2}/\chi$. The initial condition becomes

$$\Theta(\tilde{r},0) = \frac{1}{2\pi \tilde{w}_{MZ}^2}\exp\left(-\frac{\tilde{r}^2}{2\tilde{w}_{MZ}^2}\right),$$

with the dimension-less parameters :

$$\lambda = \frac{\gamma_{MCI} T_\infty E_1}{C^2 \chi n_{2D} T_a^2} \qquad \Gamma = \frac{2\gamma_d E_1}{C^2\chi n_{2D} T_a} = \frac{2\gamma_d}{\gamma_{MCI}}\frac{T_a}{T_\infty}\lambda.$$

Spatial temperature distribution $T(r,t)$ in a continuous reactive medium

$$\frac{\partial \Theta}{\partial \tau} = \lambda e^{-1/\Theta} - \Gamma \Theta + \frac{1}{\tilde{r}} \frac{\partial}{\partial \tilde{r}} \left(\tilde{r} \frac{\partial \Theta}{\partial \tilde{r}} \right),$$

- Equation similar to the one describing impulsive spot heating and thermal explosion in ordinary matter with the addition of a dimensionless damping coefficient Γ

Spatial temperature distribution $T(r,t)$ in a continuous reactive medium

$$\frac{\partial \Theta}{\partial \tau} = \lambda e^{-1/\Theta} - \Gamma\Theta + \frac{1}{\tilde{r}}\frac{\partial}{\partial \tilde{r}}\left(\tilde{r}\frac{\partial \Theta}{\partial \tilde{r}}\right),$$

- Equation similar to the one describing impulsive spot heating and thermal explosion in ordinary matter with the addition of a dimensionless damping coefficient Γ
- For a given Γ, thermal evolution is characterised only by λ_{cr}. Bifurcation between two distinct regimes : cooling ($\lambda < \lambda_{cr}$) and rapid temperature growth ("thermal runaway", $\lambda > \lambda_{cr}$)

Spatial temperature distribution $T(r,t)$ in a continuous reactive medium

$$\frac{\partial\Theta}{\partial\tau} = \lambda e^{-1/\Theta} - \Gamma\Theta + \frac{1}{\tilde{r}}\frac{\partial}{\partial\tilde{r}}\left(\tilde{r}\frac{\partial\Theta}{\partial\tilde{r}}\right),$$

- Equation similar to the one describing impulsive spot heating and thermal explosion in ordinary matter with the addition of a dimensionless damping coefficient Γ
- For a given Γ, thermal evolution is characterised only by λ_{cr}. Bifurcation between two distinct regimes : cooling ($\lambda < \lambda_{cr}$) and rapid temperature growth ("thermal runaway", $\lambda > \lambda_{cr}$)
- for a 2D system, $\lambda_{cr}(\Gamma = 0) \sim 10$, $\lambda_{cr}(\Gamma = 1.5) \sim 17$ and $\lambda_{cr}(\Gamma = 2.5) \sim 21$.

Spatial temperature distribution $T(r,t)$ in a continuous reactive medium

$$\frac{\partial \Theta}{\partial \tau} = \lambda e^{-1/\Theta} - \Gamma \Theta + \frac{1}{\tilde{r}} \frac{\partial}{\partial \tilde{r}} \left(\tilde{r} \frac{\partial \Theta}{\partial \tilde{r}} \right),$$

- Equation similar to the one describing impulsive spot heating and thermal explosion in ordinary matter with the addition of a dimensionless damping coefficient Γ
- For a given Γ, thermal evolution is characterised only by λ_{cr}. Bifurcation between two distinct regimes : cooling ($\lambda < \lambda_{cr}$) and rapid temperature growth ("thermal runaway", $\lambda > \lambda_{cr}$)
- for a 2D system, $\lambda_{cr}(\Gamma = 0) \sim 10$, $\lambda_{cr}(\Gamma = 1.5) \sim 17$ and $\lambda_{cr}(\Gamma = 2.5) \sim 21$.
- Experimental parameters$\Rightarrow$ $\Gamma \sim 2$–4 and, at threshold energy,$\lambda_{cr} \sim 10 - 30$. Good agreement with theory

Calculation vs experiments

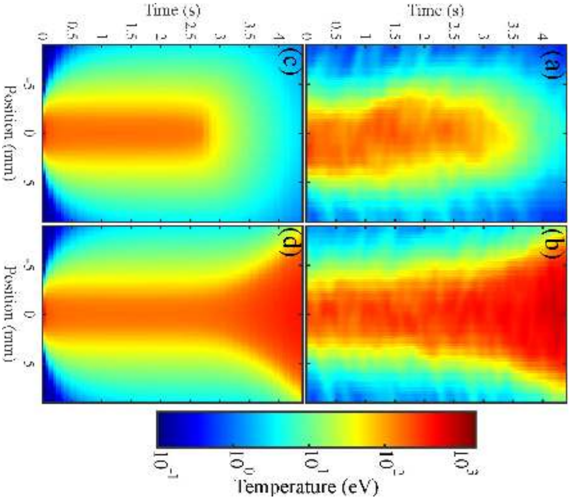

Stability of monolayer complex plasmas : Thresholds of the mode-coupling instability

State of the monolayer vs power and pressure

- Monolayer is studied under different conditions of pressure and power
- Crystalisation pressure and MCI threshold pressure are recorded

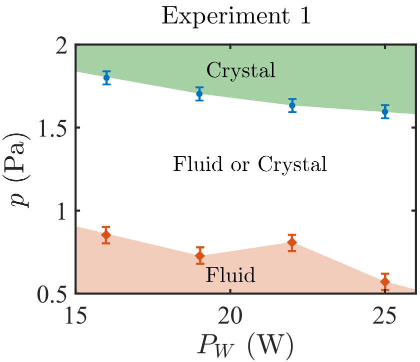

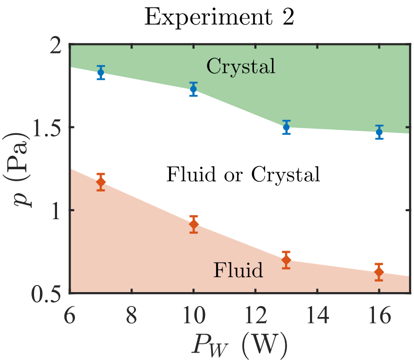

Evolution of crystal parameters

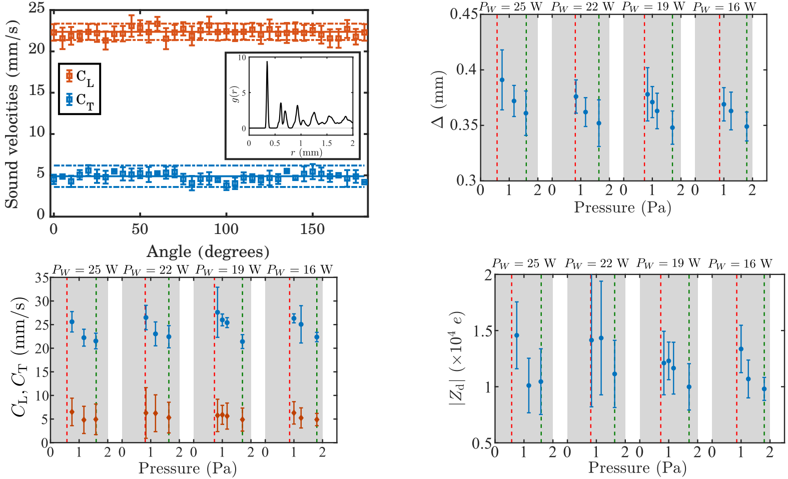

Using method described in S. Nunomura et al., Phys. Rev. Lett. **89**, 035001 (2002).

Sheath in capacitivelly coupled rf discharges

Model

Particle charge depends on local plasma parameters (T_{e}, $n_{\mathrm{i,e}}$)
Vertical confinement strength depends on sheath structure.
$\Rightarrow$ Need for proper modelling of the RF sheath :

- Collisional cold ions ($T_i = 0$ and constant ion mean free path λ_i)
- Inertia-less electrons
- No secondary electron emitted from cathode
- No ionisation in the sheath

Y. P. Raizer, et al. "Radio-Frequency Capacitive discharges" (CRC Press LLC, Florida, 1995).
M. A. Lieberman, IEEE Trans. Plasma Sci. **17**,338 (1989).
M. A. Lieberman, IEEE Trans. Plasma Sci. **16**, 638(1988).
Y. P. Song, et al. , J. Phys. D : Appl. Phys. **23**, 673 (1990).
V. A. Godyak and N. Sternberg, Phys. Rev. A **42**, 2299 (1990).
L. Couëdel and V. Nosenko, Phys. Rev. E **105**, 015210 (2022).

Experimental input

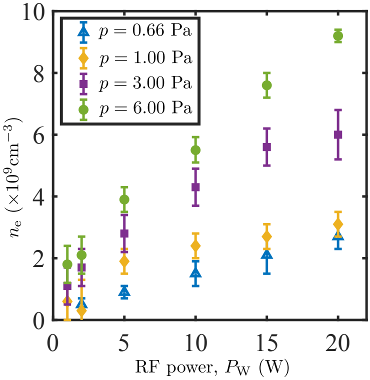

Good agreement with estimation of constant density model

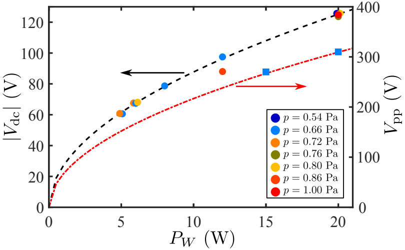

Relationship between V_{dc} and V_{pp}:

$$\frac{V_{dc}}{V_0} = \sin\left(\frac{\pi}{2}\left(\frac{A_g - A_{rf}}{A_g + A_{rf}}\right)\right)$$

In our experiment: $A_{rf} \sim 0.25 A_g$

V. Land, et al., New J. Physics **11**, 063024 (2009)

Sheath parameters as a function of pressure and power

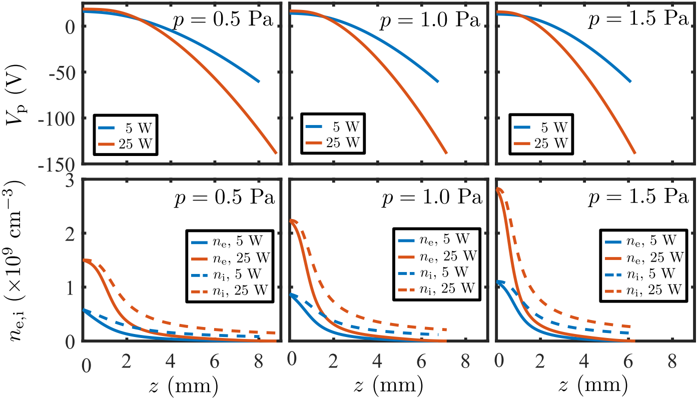

- Pressure increases ⇒ $n_{i,e}$ increases and sheath length decreases,
- Power increases ⇒ $n_{i,e}$ increase and sheath length slightly increases.

Calculated phonon spectra and MCI threshold

Z_{d}, levitation height and $f_{0_{\mathrm{v}}}$

Particle charge (Zobnin model):

$$I_{\mathrm{e}} =(-e)\cdot\sqrt{8\pi}r_{\mathrm{d}}^2 n_{\mathrm{e}} v_{T_{\mathrm{e}}}\exp(-\tilde{\varphi}), \quad (1)$$

$$I_{\mathrm{i}} =(e)\cdot\sqrt{8\pi}r_{\mathrm{d}}^2 n_{\mathrm{e}} v_{T_{\mathrm{i}}}\left(1+\tilde{\varphi}\right)\times \left[1+\frac{\tilde{\varphi}\left(\frac{T_{\mathrm{e}}}{T_{\mathrm{i}}}\frac{r_{\mathrm{d}}}{\lambda_{\mathrm{i}}}\right)}{0.07+2\left(\frac{r_{\mathrm{d}}}{\lambda}\right)+2.5\left(\frac{r_{\mathrm{d}}}{\lambda_{\mathrm{i}}}\right)+\left[0.27\left(\frac{r_{\mathrm{d}}}{\lambda}\right)^{1.5}+0.8\left(\frac{r_{\mathrm{d}}^2}{\lambda_{\mathrm{i}}\lambda}\right)\right]\frac{T_{\mathrm{e}}}{T_{\mathrm{i}}}\tilde{\varphi}+\frac{0.4\left(\frac{r_{\mathrm{d}}}{\lambda_{\mathrm{i}}}\right)^2\left(\frac{T_{\mathrm{e}}}{T_{\mathrm{i}}}\right)\tilde{\varphi}}{1-0.4\left(\frac{r_{\mathrm{d}}}{\lambda_{\mathrm{i}}}\right)}}\right], \quad (2)$$

$$Z_{\mathrm{d}} = -4\pi\epsilon_0 r_{\mathrm{d}} T_{\mathrm{e}}\tilde{\varphi}/e. \quad (3)$$

Levitation height and vertical resonance frequency:

$$Q_{\mathrm{d}}E(z_{\mathrm{lev}}) = -m_{\mathrm{d}}g, \quad (1)$$

$$\omega_v = \sqrt{\frac{|Q_{\mathrm{d}}|}{m_{\mathrm{d}}}\frac{\partial E(z)}{\partial z}}_{|z=z_{\mathrm{lev}}}. \quad (2)$$

A. V. Zobnin, et al. "Ion current on a small spherical attractive probe in a weakly ionized plasma with ion-neutral collisions (kinetic approach)", Phys. Plasmas **15**, 043705 (2008).

Z_d, levitation height and f_{0_v}

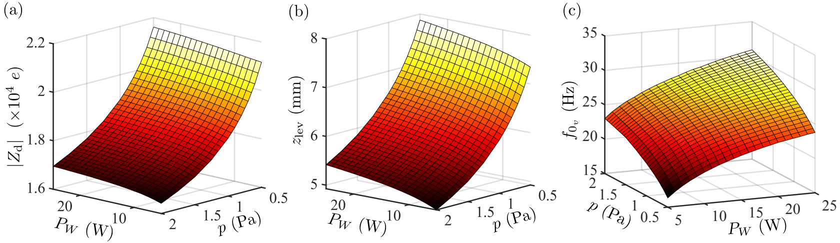

Pressure and rf power have significant influence on Z_d, z_lev and f_{0_v} :

- Power increase at constant pressure leads to increase of Z_d, z_lev and f_{0_v},
- Pressure increase at constant rf power leads to decrease of Z_d, z_lev and increase of f_{0_v}.

Mode-crossing and MCI threshold

Calculated phonon spectra.
(Zhadnov point-wake model, constant interparticle distance Δ) :

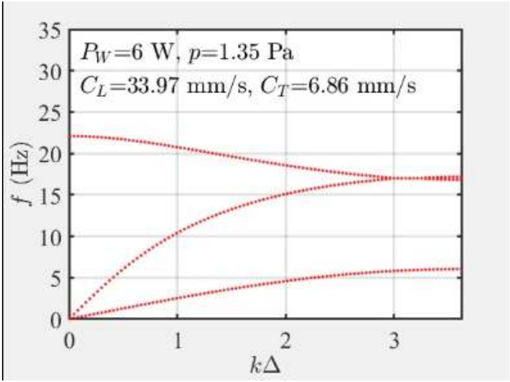

S.K. Zhdanov *et al.*, Phys. Plasmas **16**, 083706 (2009)

Mode-crossing and MCI threshold

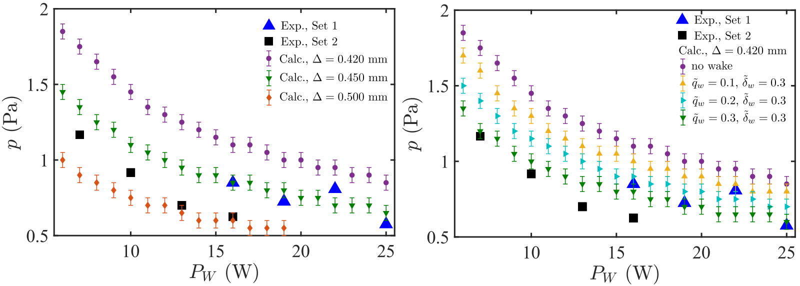

Trends for MCI threshold can be reproduced, however :

- Threshold very sensitive to interparticle distance,
- Threshold very sensitive to wake parameters.

⇒ Need proper modelling of ion wakes and confinement.

L. Couëdel and V. Nosenko, Phys. Rev. E **105**, 015210 (2022).

Sensitivity of ion wakes to plasma parameters

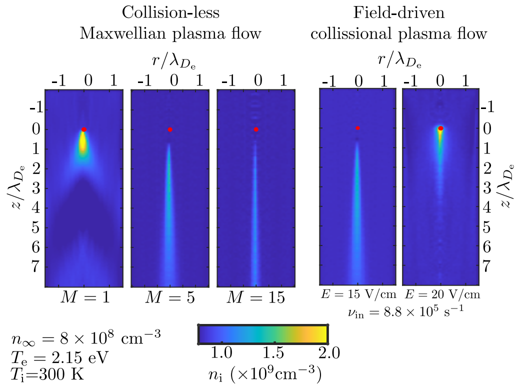

D. Kolotinskii and A. Timofeev, *OpenDust : A fast GPU-accelerated code for the calculation of forces acting on microparticles in a plasma flow.* Computer Physics Communications **288**, 108746 (2023)

Ion wakes as a function of discharge conditions

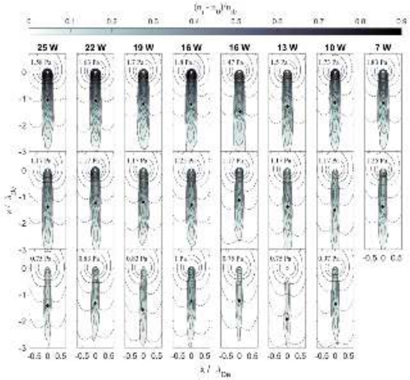

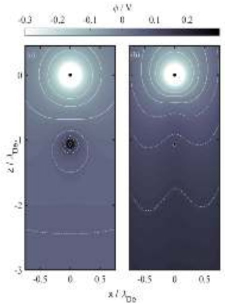

25 W, 1.58 Pa

Ion wake modelled using molecular dynamics simulation (DRIAD code) : self-consistent calculation of the ion and dust dynamics and dust charging.

R. Banka et al. "Dependence of ion wake characteristics on experimental conditions", Plasma Phys. Controll. Fus. **65**(4), 044006 (2023).

Ion wakes as a function of discharge conditions

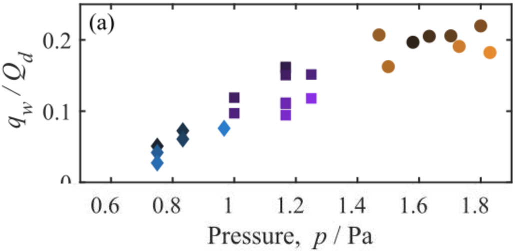

Wake charge proportional to the neutral gas pressure : ranging from $0.05 \times Q_d$ of the at $p < 1$ Pa to $0.20 \times Q_d$ at $p = 1.8$ Pa.
$\Rightarrow$ Use the obtained interaction potentials to study wave modes and MCI thresholds.

R. Banka et al. "Dependence of ion wake characteristics on experimental conditions", Plasma Phys. Controll. Fus. **65**(4), 044006 (2023).

Self-consistent wake model (Kompaneets' model)

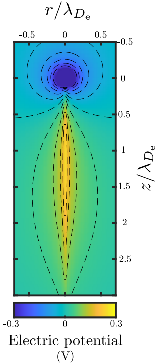

$p = 1$ Pa,
$n = 10^9$ cm^{-3},
$T_e = 3$ eV,
$Q = -15000e$.

Electric potential structure :

$$V(r,z) = \frac{Q}{2\varepsilon_0 \pi^2 l_{in}} \mathrm{Re} \int_0^\infty \mathrm{d}t \frac{\exp[it(z/l_{in}]}{1 + (l_{in}/\lambda_{sc})^2 Y(t)} \times$$

$$K_0 \left(\frac{r}{l_{in}} \sqrt{\frac{t^2 + (l_{in}/\lambda_{sc})^2 X(t)}{1 + (l_{in}/\lambda_{sc})^2 Y(t)}} \right),$$

with $X(t) = 1 - \sqrt{1 + it}$ and

$$Y(t) = \frac{2\sqrt{1+it}}{it} \int_0^1 \frac{\mathrm{d}\alpha}{[1+it(1-\alpha^2)]^2} - \frac{1}{it(1+it)}.$$

Complex potential structure with attraction at long distance.

Kompaneets et al, Phys. PLasmas **14**, 052108 (2007).

Self-consistent wake model (Kompaneets' model)

Comparison with Yukawa potential

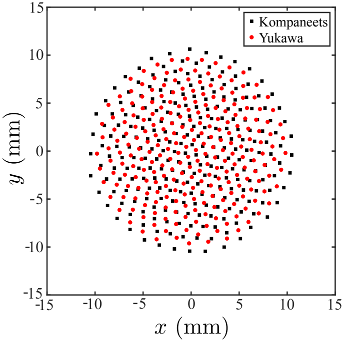

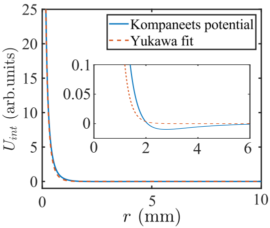

$Z_\mathrm{d} = 15000$
$f_h = 0.10$ Hz
$n_\infty = 1.0 \times 10^9$ cm^{-3}
$T_\mathrm{e} = 3$ eV, $T_\mathrm{i} = 0.027$ eV
$p = 1.0$ Pa
$l_{in} = 6.4$ mm
$E = 22$ V/cm
$M = 18.8$

Self-consistent wake model (Kompaneets' model)

Comparison with Yukawa potential

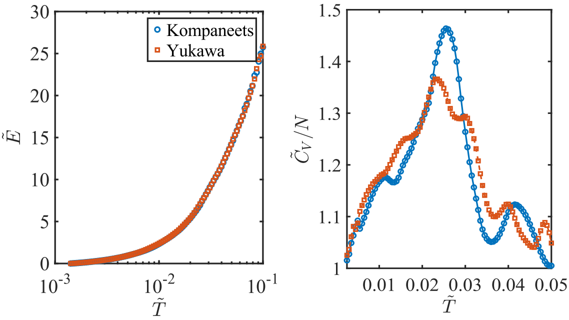

No major difference for equilibrium properties.

⇒Need to investigate MCI threshold with self-consistent interaction potentials.

Conclusion I

- Dusty plasmas are a very nice tool to study strongly coupled systems

Conclusion I

- Dusty plasmas are a very nice tool to study strongly coupled systems
- Imaging monolayer (quasi-2D) complex plasma crystal allows one to study wave propagation at the kinetic level

Conclusion I

- Dusty plasmas are a very nice tool to study strongly coupled systems
- Imaging monolayer (quasi-2D) complex plasma crystal allows one to study wave propagation at the kinetic level
- Anisotropy due to ion wakes can lead to wave-mode coupling in monolayer complex plasma crystals

Conclusion I

- Dusty plasmas are a very nice tool to study strongly coupled systems
- Imaging monolayer (quasi-2D) complex plasma crystal allows one to study wave propagation at the kinetic level
- Anisotropy due to ion wakes can lead to wave-mode coupling in monolayer complex plasma crystals
- Wave-mode coupling due to ion wakes has clear fingerprints :

Conclusion I

- Dusty plasmas are a very nice tool to study strongly coupled systems
- Imaging monolayer (quasi-2D) complex plasma crystal allows one to study wave propagation at the kinetic level
- Anisotropy due to ion wakes can lead to wave-mode coupling in monolayer complex plasma crystals
- Wave-mode coupling due to ion wakes has clear fingerprints :
  - Hybrid mode

Conclusion I

- Dusty plasmas are a very nice tool to study strongly coupled systems
- Imaging monolayer (quasi-2D) complex plasma crystal allows one to study wave propagation at the kinetic level
- Anisotropy due to ion wakes can lead to wave-mode coupling in monolayer complex plasma crystals
- Wave-mode coupling due to ion wakes has clear fingerprints :
  - Hybrid mode
  - Angular dependence

Conclusion I

- Dusty plasmas are a very nice tool to study strongly coupled systems
- Imaging monolayer (quasi-2D) complex plasma crystal allows one to study wave propagation at the kinetic level
- Anisotropy due to ion wakes can lead to wave-mode coupling in monolayer complex plasma crystals
- Wave-mode coupling due to ion wakes has clear fingerprints :
  - Hybrid mode
  - Angular dependence
  - Confinement and damping thresholds

Conclusion I

- Dusty plasmas are a very nice tool to study strongly coupled systems
- Imaging monolayer (quasi-2D) complex plasma crystal allows one to study wave propagation at the kinetic level
- Anisotropy due to ion wakes can lead to wave-mode coupling in monolayer complex plasma crystals
- Wave-mode coupling due to ion wakes has clear fingerprints :
  - Hybrid mode
  - Angular dependence
  - Confinement and damping thresholds
  - Mixed polarisation

Conclusion I

- Dusty plasmas are a very nice tool to study strongly coupled systems
- Imaging monolayer (quasi-2D) complex plasma crystal allows one to study wave propagation at the kinetic level
- Anisotropy due to ion wakes can lead to wave-mode coupling in monolayer complex plasma crystals
- Wave-mode coupling due to ion wakes has clear fingerprints :
  - Hybrid mode
  - Angular dependence
  - Confinement and damping thresholds
  - Mixed polarisation
  - Fingerprints are clearly visible on fluctuation spectra (simulations and experiments)

Conclusion II

- Experimentally demonstration of wake-mediated resonant mode coupling in a 2D plasma crystal induced by localised pulsed laser heating.

Conclusion II

- Experimentally demonstration of wake-mediated resonant mode coupling in a 2D plasma crystal induced by localised pulsed laser heating.
- Heating can trigger a rapid full melting of the crystalline monolayer.

Conclusion II

- Experimentally demonstration of wake-mediated resonant mode coupling in a 2D plasma crystal induced by localised pulsed laser heating.
- Heating can trigger a rapid full melting of the crystalline monolayer.
- Energy threshold was observed.

Conclusion II

- Experimentally demonstration of wake-mediated resonant mode coupling in a 2D plasma crystal induced by localised pulsed laser heating.
- Heating can trigger a rapid full melting of the crystalline monolayer.
- Energy threshold was observed.
- Remarkable similarities with impulsive spot heating in ordinary reactive matter.

Conclusion III

Conclusion III

- Stability of 2D complex plasma crystal with respect to MCI increases with pressure and rf power,

Conclusion III

- Stability of 2D complex plasma crystal with respect to MCI increases with pressure and rf power,
- Simple rf sheath model is able to explain the evolution of vertical confinement,

Conclusion III

- Stability of 2D complex plasma crystal with respect to MCI increases with pressure and rf power,
- Simple rf sheath model is able to explain the evolution of vertical confinement,
- MCI threshold follow the trends given by crossing of the vertical and compressional in-plane modes,

Conclusion III

- Stability of 2D complex plasma crystal with respect to MCI increases with pressure and rf power,
- Simple rf sheath model is able to explain the evolution of vertical confinement,
- MCI threshold follow the trends given by crossing of the vertical and compressional in-plane modes,
- MCI threshold very sensitive to interparticle distance and wake parameters,

Further investigations :

- Study of MCI threshold using self-consistent wake model and interactions potential obtained from simulations,
- Implementation of horizontal confinement : dependance of the interparticle distance to discharge conditions,
- Improvement of sheath model/simulations for accuracy of the MCI threshold calculation,
- Improved experimental studies of the different thresholds for various monolayer parameters and laser spot sizes (for induced melting), influence of the temperature of the fluid state on the MCI growth rate

Thank you for your attention.

Related publications :

- L. Couëdel *et al.*, Phys. Rev. Lett. **103**, 215001 (2009).
- S.K. Zhdanov *et al.*, Phys. Plasmas **16**, 083706 (2009).
- L. Couëdel *et al.*, Phys. Rev. Lett. **104**, 195001 (2010).
- L. Couëdel *et al.*, Phys. Plasmas **18**, 083707 (2011).
- T. B. Röcker*et al.*, Phys. Plasmas **19**, 033708 (2012).
- L. Couëdel *et al.*, Phys. Rev. E **89**, 053108 (2014).
- T. B. Röcker *et al.*, Europhysics Letters, **106**, 45001 (2014).
- A.V. Ivlev *et al.*, Phys. Rev. Lett **113**, 135002 (2014).
- I. Laut *et al.*, Europhysics Letters, **110**, 65001 (2015).
- A.V. Ivlev *et al.*, Phys. Rev. E **91**, 063108 (2015).
- L. Couëdel *et al.*, Europhysics Letters, **115**, 45002 (2016).
- S. O. Yurchenko *et al.*, Phys. Rev. E **96**, 043201 (2017).
- N. P. Kryuchkov,*et al.*, Phys. Rev. Lett. **121**, 075003 (2018).
- L. Couëdel *et al.*, Phys. Rev. E **97**, 043206 (2018).
- L. Couëdel and V. Nosenko, J. Imaging **5**(3), 41 (2019).
- L. Couëdel and V. Nosenko, Phys. Rev. E **105**, 015210 (2022).
- R. Banka et al., Plasma Phys. Control. Fus. **65**, 044006 (2023).